ULTRASONIC IMAGING 15, 36-47 (1993)

MODIFIED X WAVES WITH IMPROVED FIELD PROPERTIES

Tai K. Song, J-y. Lu, and J. F. Greenleaf

Biodynamics Research Unit
Department of Physiology and Biophysics
Mayo Clinic/Foundation
200 First Street SW
Rochester, MN 55905

A method to obtain a good compromise between the depth of field and the lateral resolution of "X waves" is proposed. The original X waves are theoretically nondiffracting beams generated by a specially phased infinite transmit aperture. When generated by a finite aperture, X waves are diffracting beams but have a large depth of field, maintaining uniform lateral field profiles. The proposed modification of the wave equation solution for X waves replaces a constant parameter representing the propagation angle of ultrasound with a function of radial distance at the aperture surface, and results in modified X waves that have a larger depth of field than the original X waves. Computer simulations show that a proper choice of the modification function can produce a new beam with improved field properties compared with the original X waves, promising images with higher lateral resolution and increased contrast over a large depth of field in high frame rate medical imaging. Experimental results are presented to verify the simulation results of the proposed method.

Key words: Annular array; depth of field; lateral resolution; nondiffracting beams; transmit focus; ultrasonic B-mode imaging.

I. INTRODUCTION

Recently, new classes of solutions to the scalar wave equation that governs wave propagation in isotropic/homogeneous media have been discovered, which describe nondiffracting beams [1-10] and localized waves [11]. Nondiffracting wave solutions have been studied by some investigators for applications to ultrasonic imaging [2-10]. Theoretically, these solutions represent nondiffracting beams in the sense that their spatial beam profiles do not change as they propagate. Even though these nondiffracting beams are not physically realizable, it has been shown that they can be closely approximated over a large depth of field with a finite aperture [2-10]. The resultant beams can maintain uniform lateral and axial field profiles to a certain depth, unlike conventional beams such as spherically focused beams and Gaussian shaded spherical focused beams.

The first nondiffracting solution was discovered by J. Durnin [1]. An approximation to the lowest mode of the solution, called the J_0 Bessel beam, was produced with a finite aperture acoustic device by D. K. Hsu et al. [2]. Lu and Greenleaf have closely approximated the J_0 Bessel beam with a finite aperture ultrasonic annular array transducer and suggested its application to medical imaging and tissue characterization [3-5]. Campell et al. had a similar idea to produce the J_0 Bessel beam with an acoustical annular array transducer [6]. More recently, Lu and Greenleaf have discovered families of generalized nondiffracting solutions to the isotropic/homogeneous

0161-7346/93 $5.00

scalar wave equation. One of these families represents waves that have an X-like shape in a plane along the wave axis and were termed "X waves" [7]. Some of the previously known nondiffracting waves including the J_0 Bessel beam and the plane wave are members of this family.

A generalized X wave solution is given by [7]

$$\Phi_{Xn} = e^{in\phi} \int_{-\infty}^{+\infty} B(k) J_n(kr\sin\zeta) e^{-k[a_0 - i(z\cos\zeta - ct)]}\, dk, \quad (n=0,1,2,...), \tag{1}$$

where $r = \sqrt{x^2+y^2}$ is a radial coordinate, ϕ is azimuthal angle, z is the axial distance, t is time, $B(k)$ is any well behaved complex function and could represent the system transfer function of a practical wave source, J_n is the nth order Bessel function of the first kind, $k=\omega/c$ is wave number and ω and c are angular frequency and sound speed, respectively, and a_0 and ζ are parameters which are independent of the spatial variables and time. With n=0 and $B(k)$ equal to a_0 (>0) for $k \geq 0$ and 0 for $k<0$, we obtain the zeroth order broadband X wave, Φ_{XBB_0}, which has a peak intensity on the wave center and is axially symmetric [7]

$$\Phi_{XBB_0} = \frac{a_0}{\sqrt{(r\sin\zeta)^2 + [a_0 - i(z\cos\zeta - ct)]^2}}. \tag{2}$$

For a bandlimited $B(k)$ a bandlimited X wave is calculated as

$$\Phi_{XBL_0} = \mathbf{F}^{-1}[B(k)] * \Phi_{XBB_0}. \tag{3}$$

where * denotes the time convolution and $\mathbf{F}^{-1}$ represents the Fourier inverse transformation.

The X waves described by Eqs. (1) and (2) with same transversal intensity field profile at any depth cannot be realized exactly because each spectral component of Eq. (1) has a finite energy over an entire transversal plane. However, it was shown that they can be physically approximated in a finite region by truncating and driving Eq. (1) with a finite aperture at source plane (z=0) [7]. These X waves generated by a finite aperture are of practical importance in two aspects when applied to ultrasonic imaging. First, they can provide much larger depth of field in B-scan imaging than conventional beams. Second, they should be very useful for tissue characterization because the diffraction correction process normally required may be negligible due to their minimally diffracting properties. For medical imaging applications, however, they have practical problems, e.g., high sidelobe level and the tradeoff between depth of field and lateral resolution. The most convenient way to reduce the high sidelobes may be to increase ζ because the magnitude of Eq. (2) decays faster for a larger ζ. However, large increases in ζ cannot be made because the depth of field of X waves decreases with ζ. This paper focuses on reducing the lateral beamwidth and sidelobe levels of X waves for medical applications without sacrificing depth of field.

One of the authors (Song) found that if the parameter, ζ, in Eq. (1) is modified as a function of the radial distance, r, i.e., $\zeta = \zeta(r)$, on a transducer surface in a manner similar to that used in some axicons [12-14], the resultant beams have larger depth of field with improved lateral field profile at near and far depths. One of the other authors (Lu) suggested a modification function expressed by,

$$\zeta(r) = \zeta_0 - \zeta_1 (r/a)^m, \; 0 \leq r \leq a, \; (m \geq 0), \tag{4}$$

where ζ_0 and ζ_1 are constants and a is the radius of aperture. Computer simulations have shown

that m=1/2 provides a reasonable compromise between the depth of field and lateral resolution. Because the modified X waves ($m \neq 0$) provide reduced lateral beamwidths and sidelobes compared with the original X waves ($m = 0$) within the same depth of field, as will be shown by simulations and experiments in Sections III and IV, the applicability of X waves in medical ultrasonic imaging becomes more promising. When multiple sequential transmit foci can not be employed to increase the depth of field of conventional focused beams because of high frame rates, modified X waves may be able to provide high resolution and contrast images throughout the region of interest.

II. TRADEOFF IN FIELD PROPERTIES OF X WAVES

The field magnitude of broadband X waves is calculated from Eq. (2) as

$$|\Phi_{XBB_0}| = \frac{a_0}{\{[a_0^2 + (r\sin\zeta)^2 - (z\cos\zeta - ct)^2]^2 + 4a_0^2(z\cos\zeta - ct)^2\}^{1/4}}. \tag{5}$$

The snapshot lateral field response (measured at $ct = z\cos\zeta$) is given by

$$|\Phi_{XBB_0}|_s = \frac{a_0}{\sqrt{a_0^2 + (r\sin\zeta)^2}}. \tag{6}$$

X waves have peak lateral field response on their X-branches [7]. The X-branches of Eq. (5) can be obtained by solving

$$\frac{\partial}{\partial t}|\Phi_{XBB_0}| = 0, \tag{7}$$

which gives

$$ct = z\cos\zeta \pm \sqrt{(r\sin\zeta)^2 - a_0^2}, \quad |r\sin\zeta| > a_0. \tag{8}$$

On the X-branches, the peak lateral field response is

$$|\Phi_{XBB_0}|_p = \sqrt{a_0/2|r\sin\zeta|}. \tag{9}$$

Equations (6) and (9) show that both the snapshot and peak lateral field responses decay with r at a rate increasing with ζ. Therefore, there is a tradeoff between depth of field and lateral resolution when a finite aperture is used to produce X waves, because the maximum depth of field of X waves is determined by [7],

$$z_{\max} = \frac{a}{\tan\zeta}, \tag{10}$$

where a is a radius of aperture. Decreasing ζ to obtain a larger depth of field broadens the lateral beamwidth.

In this paper, we suggest a simple method to optimize this tradeoff. A finite aperture driven with a source distribution expressed by Eq. (1) with $\zeta = \zeta(r)$ generates modified X waves that also

have an X-like shape but provide larger depth of field and better lateral field intensity profiles at near and far depths than the original X waves. In the following simulations and experiments, only the peak lateral field intensities along the X-branches will be examined because these contain the highest and most slowly decaying profiles.

III. MODIFIED X WAVES

The original X waves are physically generated by a finite aperture with a source distribution of Eq. (1) with a constant ζ which corresponds to $m = 0$ in Eq. (4). For nonzero m's, Eq. (1) produces different wave fields, which we will call modified X waves. The field distributions of the original and modified X waves generated by a finite aperture were calculated by using the Rayleigh-Sommerfeld formula [15]. The source distribution, Φ_{Ms}, for any $\zeta(r)$ is obtained by substituting z = 0 and n = 0 into Eq. (1), giving

$$\Phi_{Ms}(r, \frac{\omega}{c}) = B(\frac{\omega}{c}) J_0(\omega r \sin\zeta(r)/c)\, e^{-ka_0} \cdot \Pi(\frac{r}{2a}). \tag{17}$$

where $\Pi(s)$ is a rectangular function which is 1 when $|s| \leq 1/2$ and 0 otherwise.

The field distribution in absorption free, homogeneous media is calculated as

$$\Phi_M(z, r, t) = \int_{-\infty}^{+\infty} d\omega\, e^{-i\omega t} \frac{1}{i\lambda} \int_0^a \int_0^{2\pi} \Phi_{Ms}(r_0, \omega/c) e^{ikR} \frac{z}{R^2} r_0 dr_0 d\phi, \tag{18}$$

where R is a distance between a source point and an observation point.

Figures 1 and 2 are beam plots of the simulation results for the original bandlimited zeroth order X wave (n,m = 0) and the modified X waves (n = 0, m $\neq$ 0) produced by a finite aperture. In this simulation, $B(\omega)$ was assumed to have the form of a Blackman window function [7] with a central frequency of 2.5 MHz and a -6 dB one way bandwidth of 2 MHz. From figures 1 and 2(b), we can see that the lateral beamwidth is smaller for a larger m when z/D $\leq$ 4. On the contrary, at far depths (z/D $\geq$ 6), the lateral beamwidth is smaller for a smaller m. This means that the nondiffracting property seems to be better preserved for a smaller m, which can be explained from figure 2(a). In this figure, the peak on-axis field amplitude decays faster for a larger m, where it is almost unchanged in a certain region, z/D $\leq$ 3.5, for m = 0. In this region, the original X wave has uniform 6 dB lateral beamwidth as can be seen from figure 2(b). Deeper than this region, however, the on-axis peak for m = 0 starts to fall off and reaches -6 dB at the point defined as the maximum depth of field calculated by Eq. (10) [7]. Among the modified X waves, m=1/2 gives larger -6 dB depth of field that is much larger than that of the original X wave and has less change in 6 dB lateral beamwidth (Fig. 2). As a result, the modified X wave for m=1/2 provides larger depth of field with narrower lateral beamwidth at near depth and lower sidelobes at far depths than the original X wave, as can be seen from figures 1 and 2. From these results, we can conclude that modifying the X wave with m=1/2 provides a very good compromise between depth of field and lateral beamwidth.

The sidelobes of the X waves in figure 1 are relatively high for medical imaging applications and increase suddenly around certain lateral distances, which can result in low contrast images. The easist way to reduce the sidelobe levels of X waves may be to raise the values of $\zeta(r)$. This is because both the snapshot and peak lateral field responses decay faster for a larger ζ as can be seen from Eqs. (6) and (9). For medical B-scan applications, the constant $\zeta(r) = \zeta_0 - \zeta_1$ for the ori-

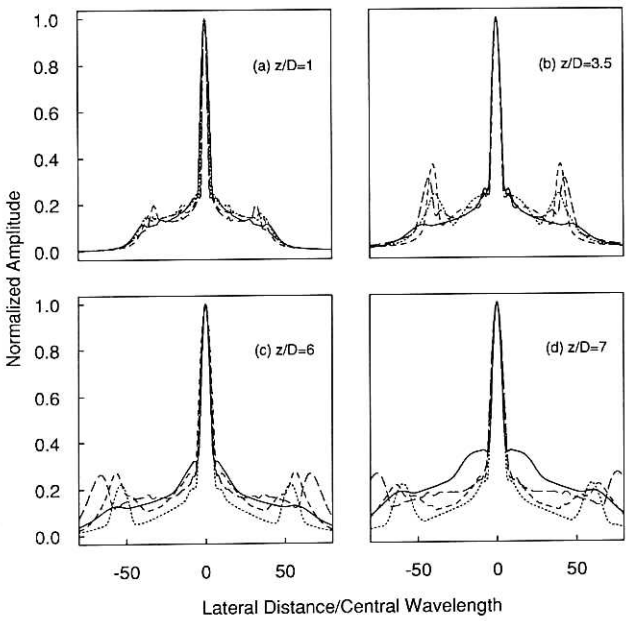

Fig. 1 Comparison between the peak lateral field amplitude profiles along the X-branches of original and modified X waves at several f-numbers (f=z/D, where z and D are the axial distance and the diameter of the transducer). Solid, dotted, short dashed, and long dashed lines correspond to the original X waves (m = 0), modified X waves with m = 1/2, 1, and 2, respectively. f_0 = 2.5 MHz, $\zeta_0 = 8^o$, $\zeta_1 = 4^o$, a_0 = 0.01, and D = 5 cm.

ginal X wave (m=0) can be increased to 7^o (z_{max} = 20.3 cm) for a finite aperture to obtain a depth of field of 20 cm. However, $\zeta 0$ and ζ_1 for modified X waves can be chosen larger than 7^o to further reduce the mainlobe width and sidelobe levels because the modified X wave has a larger

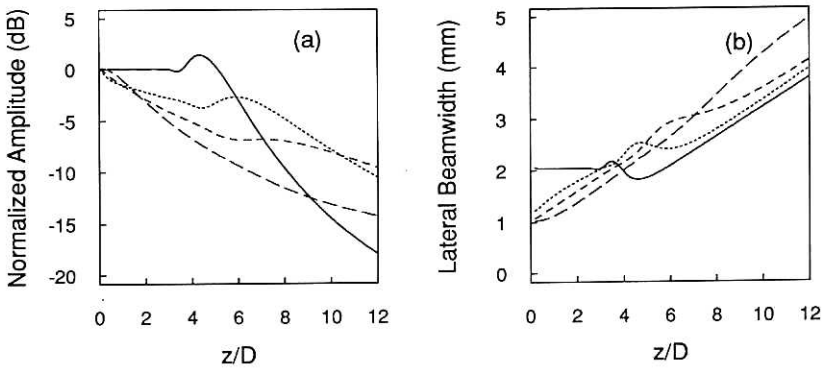

Fig. 2 Plots for (a) normalized peak on-axis field amplitude and (b) 6 dB lateral beamwidth (HWHM) of the X waves in figure 1. Solid, dotted, short dashed, and long dashed lines correspond to m = 0, 1/2, 1, and 2, respectively.

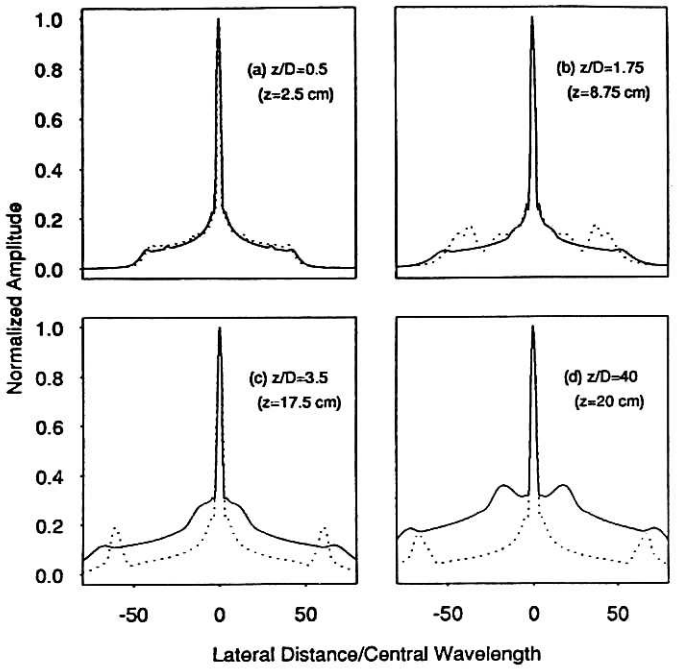

Fig. 3 Comparison between the peak lateral field responses of the original (solid line) and the proposed X wave (m=1/2, dotted line) at four depths for f_0 = 3.5 MHz, $\zeta_0 = 16^o$, $\zeta_1 = 8.2^o$, a_0 = 0.01, and D = 5 cm. Modified X wave provides a larger depth of field.

depth of field than the original X wave for the same values of ζ_0 and ζ_1, as was shown in figure 1. Figure 3 shows the lateral field profiles of the modified X wave (m=1/2) with $\zeta_0 = 16^o$ and $\zeta_1 = 8.2^o$ compared with an X wave with m = 0 and $\zeta = \zeta(r) = 8.2^o$. Due to the increased ζ (=8.2^o), the X waves show narrower lateral beamwidths in figure 3 than in figure 1. In figure 3, we can also see the same advantage of the modified X wave as shown in figure 1. The X wave with m=0 shows high sidelobes at z = 17.5 and 20 cm because these depths exceed its depth of field, z_{max} = 17.4 cm. On the contrary, the modified X wave (m=1/2) has a fast decaying lateral field profile even at z = 20 cm.

The sidelobe levels of the modified X wave with m=1/2 in figure 3 can be further reduced if dynamic Gaussian shaded focus is used in receive. In this case, the sidelobe peaking would not cause serious problems in imaging since it occurs relatively far from the center axis: for example, when nonshaded dynamic focus is used in receive, the lateral distance to the first null point of the receive field response is $1.22\lambda z/D$ [15], 2.135×(central wavelength) at z = 8.75 cm (Fig. 3(b)), while the sidelobe peaking at the same depth occurs at 37×(central wavelength).

IV. EXPERIMENTS

A block diagram of the experimental system for modified X waves is shown in figure 4. An ultrasonic annular array transducer made of PZT ceramic/polymer composite material was used to

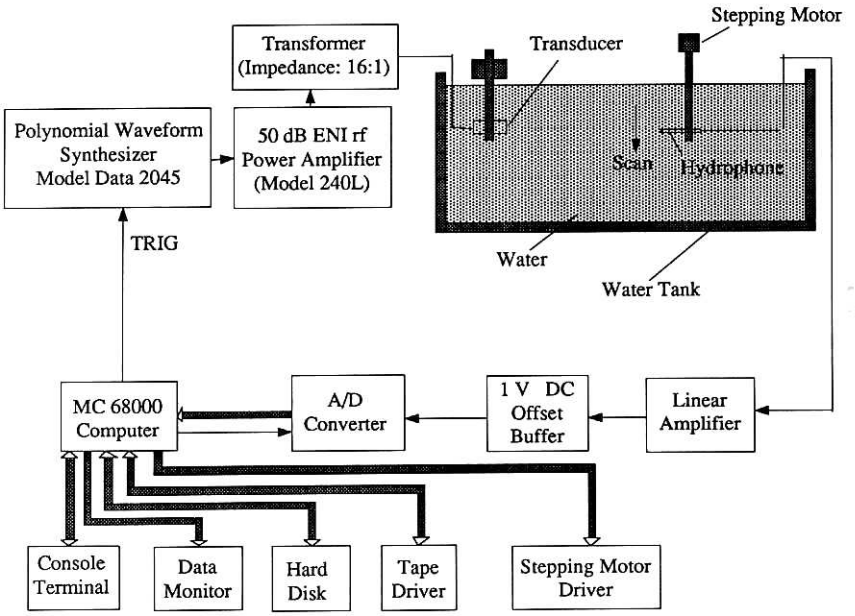

Fig. 4 Block diagram of experimental system for automatically measuring the pulsed acoustic fields of X waves generated by a 10-element annular array transducer.

produce the modified X waves [3,7,8]. The transducer has 10 elements with a diameter of 50 mm. Its central frequency is 2.5 MHz and the -6 dB two way (pulse-echo) bandwidth is about 50 % of the central frequency. A polynomial waveform generator (Model 2045, Analogic, Peabody, MA) was used to produce the waveforms. To cover the whole frequency range of the transducer and program the waveform generator with a closed form expression, a broadband X wave solution of Eq. (2) was with a small a_0 (= 0.05 mm). The waveforms for m = 0 and 1/2 were calculated by setting z = 0 in Eq. (2) for $-5\ \mu s \le t \le +5\ \mu s$. The parameters were set to $\zeta_0 = 8^o$, $\zeta_1 = 4^o$, and the radius of aperture, a = 25 mm. The radial distance, r, for the calculation of the drive waveform of each transducer element is set to the average radius of that element. The drive waveforms were amplified by a 50 dB rf power amplifier (Model 240L, ENI, Rochester, NY) and connected to the corresponding transducer elements through 16:1 impedance reduction transformers to ensure waveform fidelity. The acoustic pressure field in water was measured with a 0.5 mm diameter hydrophone (Model NP-1000, NTR systems, Seattle, WA) in a plane along the axis of the transducer and superposed over the 10 transducer elements in a computer. The scan of the hydrophone was synchronized to the excitation of the acoustic waves and controlled by a minicomputer. The received signals were amplified, digitized, and sent to a Sun workstation for further processing. The field profiles were obtained by superposition of rf field profiles resulting from each individual element.

Figure 5 shows the simulation results of the X waves (m = 0, 1/2) for the parameters described above produced by a continuous aperture. Simulation of a 10-element annular array transducer is shown in figure 6. In figure 5, we can see that the modified X wave has a smaller lateral beamwidth at near depth (z/D=1) and reduced sidelobe level at far depth (z/D=7) than the original X wave. The -6 dB depth of field of the modified X wave is increased about 23% compared with that of the original X wave. In figure 6, the piecewise approximation by an actual annu-

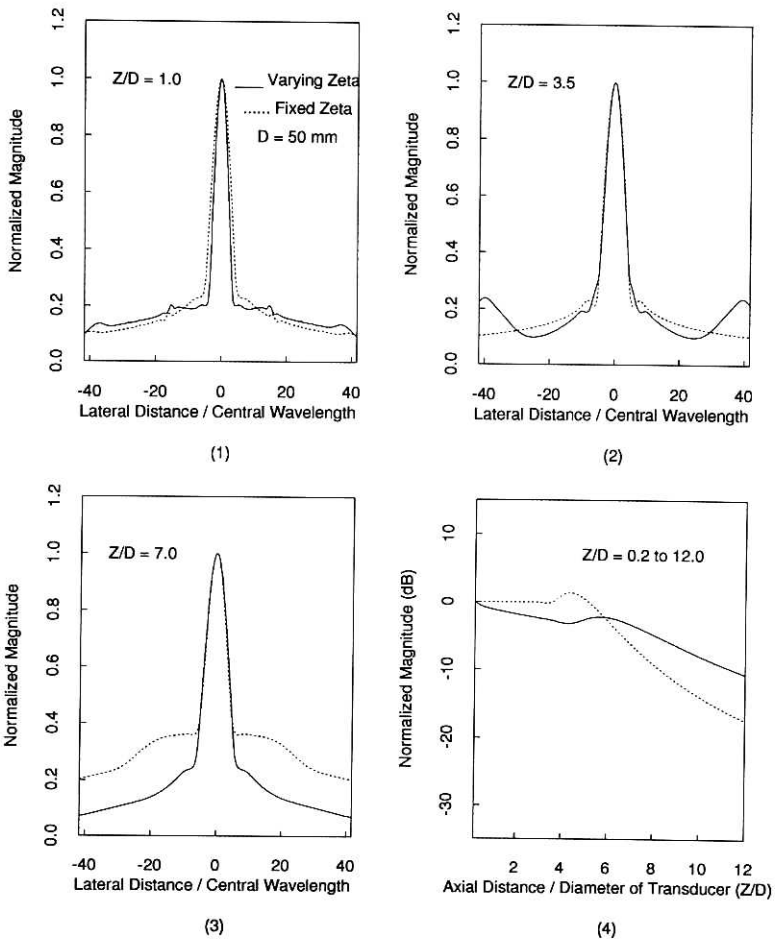

Fig. 5 Simulated beam plots of the original X wave (m = 0, dotted line) and modified X wave (m = 1/2, solid line) for parameter values used in experiment (assuming no array quantization, i.e., by a continuous aperture). Panel (1) to (3) represent the peak lateral field amplitude plots along the X-branches at different depths and panel (4) represents the peak on-axis field amplitude profile.

lar array transducer shows a stronger influence when z/D is small. This array quantization effect would be reduced by an annular array with more elements. The experimental results in figure 7 show a good agreement with simulation results in figure 6. The small differences between simulations and experiments could be caused by our assumption in simulations that the transducer transfer function, $B(k)$, was a Blackman window.

V. SUMMARY

It was shown in figures 1 and 3 that modified X waves with m=1/2 provide a better field profile compared with the original X wave improving the potential advantage of X waves in ultra-

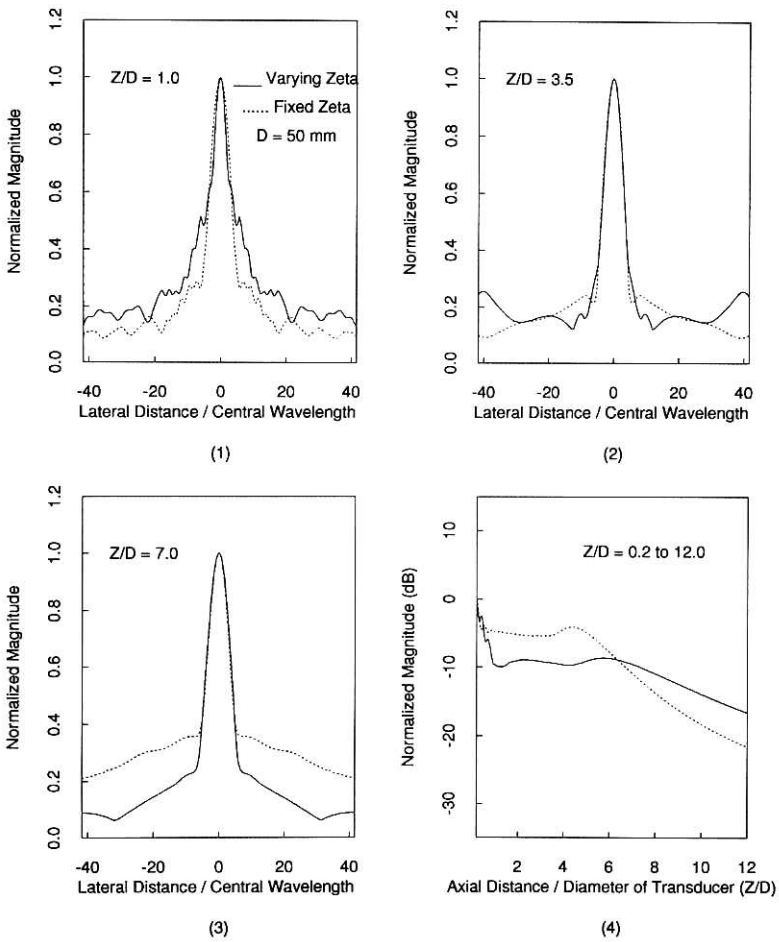

Fig. 6 Beam plots of the same X waves in figure 5 simulated with a 10-element annular array modeling the physical array used in the experiment reported in figure 7. Panels and lines are identical to those in figure 5.

sonic imaging. The peak on-axis field amplitude of the modified X wave decays more slowly at large depths than the original X wave and so reaches to -6 dB at a farther depth, as can be seen in figure 2(a)), which means that the modified X wave has a larger depth of field. Hence, the sidelobes of modified X waves at long depths (panels (c) and (d) in figures 1 and 3) are much less than those of original X waves at long depths while the mainlobe widths are slightly larger. In addition, the modified X wave has narrower lateral beamwidths at short depths, as can be seen in figure 2(a). In figure 3(a), which shows the field responses of X waves with larger $\zeta(r)$ for medical applications, the -6 dB lateral beamwidth was 1.51 mm for original X wave and 1.45 mm for the modified X wave.

The modified X wave with m=1/2 was experimentally produced in figure 7, which shows a good agreement with corresponding simulation results shown in figure 6. In this experiment, we calculated the drive waveform of each transducer element according to Eq. (2). However, the actual

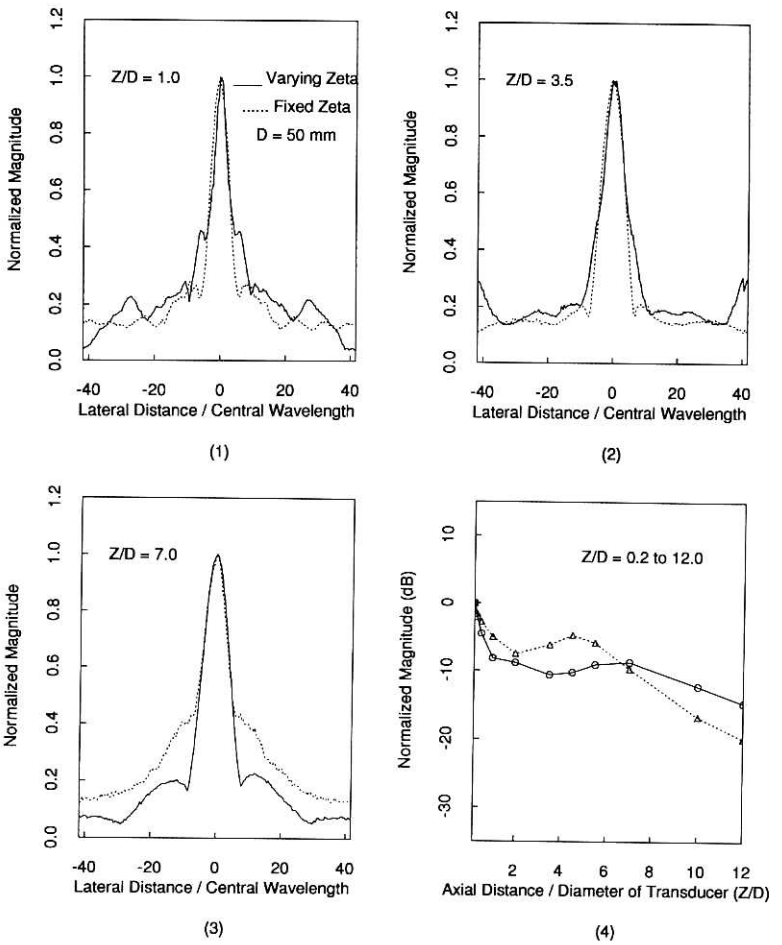

Fig. 7 Beam plots of the X waves corresponding to figure 6 which were generated and measured by the experimental system of figure 4. The triangular and circular marks in panel (4) represent the points where the peak on-axis field amplitude were measured.

radiated waveforms from the surface of the transducer will be different from the theoretically calculated ones due to the overall transfer function of the transmitting system for our experiments, which includes the electric response of the transmitting circuit and the electromechanical response of the transducer. That is, the actual transfer function, B(k), differs from a Blackman window function used as an overall transfer function in our simulations. The difference between the actual and assumed transfer functions would cause the difference between the simulated and experimental field patterns but may not pose a problem from the imaging point of view because B(k) does not affect the basic properties of X waves determined by Φ_{XBB_0} in Eq. (3). Actually, the experimental beam plots in figure 7 did not show noticeable difference from the simulated ones in figure 6. More details regarding the physical realization of X waves have been reported in our previous articles [8-10].

Both in figures 6 and 7, the sidelobe levels of the modified X wave are reduced at long depth (z/D=7). At near depth (z/D=1), however, we cannot see any indication of reduced lateral beam width that is observed in figure 5. This is because of the piecewise approximation of the driving waveforms by a ten element annular array. From figures 5 and 6, we can be see that the piecewise approximation shows a stronger influence at shorter depth and for larger ζ (the modified X wave can be thought to have larger ζ at near depths). Because the simulation and experimental results are very close (Figs. 6,7), however, one can easily find by simulation how many elements are needed to produce the X wave with a desired accuracy at short depths with a given aperture size.

From the above discussions, it can be concluded that the modified X wave provides a good compromise between the depth of field and lateral resolution of the original X wave. Since the modified X wave provides a larger depth of field, we could increase ζ_0 and ζ_1 higher than the constant ζ for the original X wave to reduce lateral beamwidth and sidelobe level without sacrificing depth of field. We expect that the combined use of the modified X wave and dynamic receive focus could provide a high resolution and high contrast image over a larger depth of field than conventional focused beams in high frame rate B-scan imaging (that is, when sequential transmit focus can not be used), because the conventional transmit beams focused at only one point diverge quickly from the focal point.

ACKNOWLEDGMENTS

The authors appreciate the help of Thomas M. Kinter in developing software for data acquisition and Randall R. Kinnick in making an experimental circuit for transducer excitation. The authors also appreciate the secretarial assistance of Elaine C. Quarve and the graphical assistance of Christine A. Welch. This work was supported in part by grant CA43920 and CA54212-01 from the National Institute of Health.

REFERENCES

[1] Durnin J., Exact solutions for nondiffracting beams. I. The scalar theory, *J. Opt. Soc. Am. 4*, 651-654 (1987).

[2] Hsu D.K., Margetan F.J., and Tompson D.O., Bessel beam ultrasonic transducer: Fabrication method and experimental results, *Appl. Phys. Lett. 55*, 2066-2068 (1989).

[3] Lu J-y. and Greenleaf J.F., Ultrasonic nondiffracting transducer for medical imaging, *IEEE Trans. Ultrasonics, Ferroelectr., Freq. Control UFFC-37*, 438-447 (1990).

[4] Lu J-y. and Greenleaf J.F., Pulse-echo imaging using a nondiffracting beam transducer, *Ultrasound in Med. Biol. 17*, 265-281 (1991).

[5] Lu J-y. and Greenlcaf J.F., Evaluation of Nondiffracting Transducer for Tissue Characterization, in *1990 IEEE Ultrasonic Symposium Proc.*, pp. 763-765 (IEEE Cat. No. 90CH 2938-9).

[6] Campbell J.A. and Soloway S., Generation of a nondiffracting beam with frequency independent beamwidth, *J. Acoust. Soc. Am. 88*, 2467-2477 (1990).

[7] Lu J-y. and Greenleaf J.F., Nondiffracting X waves–Exact solutions to free-space scalar wave equation and their finite aperture realizations, *IEEE Trans. Ultrasonics, Ferroelectr., Freq. Control UFFC-39*, 19-31 (1992).

[8] Lu J-y. and Greenleaf J.F., Experimental verification of nondiffracting X waves, *IEEE Trans. Ultrasonics, Ferroelectr., Freq. Control UFFC-39*, 441-446 (1992).

[9] Lu J-y. and Greenleaf J.F., Theory and Experiments of Nondiffracting X Waves, in *IEEE 1991 Ultrasonics Symposium Proc.*, pp. 1155-1199 (IEEE Cat. No 91CH 3079-1)

[10] Lu J-y. and Greenleaf J.F., Diffraction-limited Beams and their Applications for Ultrasonic Imaging and Tissue Characterization, in *New Developments in Ultrasonic Transducers and Transducer Systems*, F.L. Lizzi, Ed., *Proc. SPIE 1733*, pp. 92-119 (1992).

[11] Ziolkowski R.W., Lewis D.K., and Cook B.D., Evidence of localized wave transmission, *Phys. Rev. Lett. 62*, 147-150 (1989).

[12] Dietz D.R., Apodized conical focusing for ultrasound imaging, *IEEE Trans. Sonics Ultrasonics SU-29*, 128-138 (1982).

[13] Murphy R.V., Toroidal, conical and spherical lenses in ultrasonic inspection, *Mater. Eval. 39*, 391-395 (1981).

[14] O'donnell M., A proposed annular array imaging system for contact B-Scan applications, *IEEE Trans. Sonics Ultrasonics, SU-29*, 331-338 (1982).

[15] Goodman J.W., *Introduction to Fourier Optics* (Mcgraw-Hill, New York, 1968).